Soft-mode dynamics in micrograin and nanograin ceramics of strontium titanate observed by hyper-Raman scattering

B. Hehlen,[1,2] A. Al-Zein,[3,*] C. Bogicevic,[3] P. Gemeiner,[3] and J-M. Kiat[3,4]

[1]*Université Montpellier 2, Laboratoire Charles Coulomb UMR 5221, F-34095 Montpellier, France*

[2]*CNRS, Laboratoire Charles Coulomb UMR 5221, F34095 Montpellier, France*

[3]*Laboratoire Structures, Propriétés et Modélisation des Solides, Ecole Centrale Paris, CNRS UMR 8580, Grande Voie des Vignes, 92295 Chatenay-Malabry Cedex, France*

[4]*Laboratoire Léon Brillouin, CE Saclay CNRS UMR 12, 91991 Gif-Sur-Yvette Cedex, France*

(Received 12 October 2012; revised manuscript received 20 December 2012; published 22 January 2013)

The low-frequency vibrations of micro- and nanograin ceramics of strontium titanate are investigated by hyper-Raman spectroscopy. The combination of a confocal optical microscope with an ultranarrow Notch filter enabled an accurate spectroscopy on both the Stokes and anti-Stokes side down to about 8 cm^{-1}. A splitting of the soft mode into E_u- and A_{2u}-symmetry vibrations is clearly observed in the micrograin sample. The peculiar temperature dependence of $\omega^2_{A_{2u}} - \omega^2_{E_u}$ emphasizes a nonlinear coupling between the square of the TiO_6 tilting angle and the spontaneous strain $c/a - 1$. In addition, the very different temperature behavior of the linewidth of the two soft components is assigned to the growth of a disorder anisotropy on cooling, probably on the titanium site.

DOI: 10.1103/PhysRevB.87.014303 PACS number(s): 77.80.−e, 63.20.−e, 78.30.−j

I. INTRODUCTION

$SrTiO_3$ (STO) was widely studied in the 1970s partly as a textbook example of second-order displacive transition, namely its cubic ($Pm\bar{3}m$) to tetragonal ($I4/mcm$) instability at $T_a = 105$ K.[1,2] The primary order parameter is the staggered rotation angle φ, but the transition also induces a spontaneous strain, $c/a - 1$, sometimes referred as the secondary order parameter, originating from the growth of the c-tetragonal axis.[3,4] At lower temperature a ferroelectric instability is prevented by zero-point quantum fluctuations of the ions. As a consequence, the dielectric constant continuously increases and saturates at low temperature at a very high value ∼24 000 in the single crystal.[5] A ferroelectric state can be induced by doping impurities,[6] under electric field,[7] applied pressure,[8] isotopic substitution,[9] etc., indicating the highly unstable character of STO with regards to ferroelectricity.

STO, as well as many other compounds in the oxide perovskite family, benefited from a renewed interest, thanks to recent issues related to finite-size effects and their influence on ferroelectricity, for example in nanoparticles with controlled grain size. These works were motivated by both fundamental and applied concerns. One limitation for applied devices is the strong reduction of ϵ in compressed powders and ceramics when the grain size is reduced.[10] A possible interpretation is given by the core-shell model. The latter supposes that the grain is composed of a core having the properties of the bulk material embedded by one (or two) shell(s) having a very low dielectric constant, ∼10–100, and a typical thickness of 1 nm.[11,12] The shell is structurally distorted, e.g., by oxygen vacancies, extra atomic species arising from the synthesis, nonstochiometry, and off-centered atomic displacements, leading to a frozen polarization and strong local stresses. Both limit the growth of the effective dielectric constant and moreover affect the core properties. Consequently, these extrinsic effects mask the ultimate dielectric and polarization properties of the nanosystems.

From the point of view of the vibrations, the antiferrodistortive transition at T_a is controlled by a zone-boundary soft mode associated with the librations of the TiO_6 octahedra.[2] The mode appears at zone center in the tetragonal phase owing to the doubling of the unit cell. It splits into A_{1g}- and E_g-symmetry vibrations, corresponding to librations along the c axis and along the two fourfold axes of the (a,b) plane, respectively. Similarly, in the single crystal the three polar F_{1u} vibrations of the cubic phase split into A_{2u} and E_u modes. The $A_{2u} + E_u$ doublet of lowest frequency corresponds to the soft mode, in which the central Ti ion moves with respect to the oxygen cage, either along the c axis (A_{2u}) or in the (a,b) plane (E_u). Their temperature dependence mimics the behavior of the inverse dielectric constant and therefore saturates at very low frequency on cooling, 16.5 cm^{-1} and 7.8 cm^{-1}, respectively.[13,14] In STO ceramics, polar modes are observed in Raman scattering (RS) although they are forbidden by symmetry. The signal likely arises from distorted regions with local loss of inversion center in which the selection rules are lifted.[11] The polar modes can also be investigated by infrared spectroscopy (IR). In that case, the excitation wavelengths are much larger than the grain size, and it is possible within the effective medium approximation (EMA) to relate the soft-mode response to the macroscopic permittivity.[12]

In the context described above, hyper-Raman scattering[15] provides an interesting alternative to study the vibrations of ferroelectric materials,[13,14,16,17] particularly in ceramics. One main interest arises from its selection rules which are different from those of RS. In particular, transverse (TO) and longitudinal (LO) components of polar modes are always active in hyper-Raman scattering (HRS) whatever the crystal symmetry. In other words, contrary to Raman, the polar modes of STO scatter in HRS through an allowed scattering process and should be more representative of the polar state of the undistorted (core grain) regions. Moreover, the excitation wavelength is usually comparable to the grain sizes, and one therefore expects the EMA not to apply. Accordingly, the spectroscopy should be more sensitive to microscopic than to macroscopic properties. In HRS, the modes can be followed down to very low frequency provided the hyper-Rayleigh line at $\omega = 0$ is efficiently filtered out. It is this intense elastic

contribution associated with very weak hyper-Raman efficiencies due to low damage thresholds that up to now prevented performing the spectroscopy in ABO_3-type ceramics.

The technical improvements which made this study feasible and the sample description are detailed in the next section. Room temperature data are presented in Sec. III while the temperature dependence of the soft modes in the different samples is discussed in Sec. IV. Finally, the main findings are summarized in Sec. V.

II. EXPERIMENTAL DETAILS

HRS is excited by a Nd-YAG pulsed laser emitting at $\lambda = 1064$ nm with 5 kHz repetition rate and ~40 ns pulsed width.[18] The incident radiation is focused into the sample by the ×20 objective of an optical microscope,[19] leading to a waist diameter of about 10 μm. HRS under an optical microscope is essential for ceramic investigations, because objectives reduce the depth of field and therefore optimize the efficiency of the scattering process in case of nontransparent materials. The backscattered light at wavelengths around that of the hyper-Rayleigh line, i.e., $\lambda = 532$ nm, is subsequently analyzed by a single-grating diffractometer of $f = 640$ mm focal length and 1800 (or 600) grooves/mm. A confocal setup is positioned on the scattered light trajectory. It makes a magnified image of the scattering volume into holes of adjustable diameters. The latter range from 20 μm to 200 μm, improving thereby the definition of the scattering volume, in particular with regards to its depth. With a 20 μm hole one reaches spatial resolution of few μm^3 but at the expense of a strong intensity reduction. Another effect of the confocal setup is to filter the elastic signal (hyper-Rayleigh) arising from the surrounding of the scattering volume. This is very efficient even for the largest hole, for which the latter is reduced by a factor of ~10 while the inelastic component only decreases by 2.5. To further reduce the strong elastic component, we positioned a Notch filter with an ultranarrow bandwidth[20] of 5 cm^{-1} (HWHM) on a parallel path of the scattered beam. It has a transmission >90% and an optical density of 4 which is reached in case of weakly diverging beams. The association of the two devices described above keeps out about 10^4–10^5 of the elastic intensity, and opens the possibility of measuring the inelastic signal down to ±8 cm^{-1} in STO nanoparticles and ceramics.

Three samples have been investigated. They have been obtained by different thermal treatments of the same STO powder of 15 nm grain size. The latter was prepared by the ball milling method in a ZrO_2 bowl using micrometric powder of STO as starting material. Two pellets were prepared by uniaxial pressure of 40 MPa at room temperature and then isostatic compaction at 750 MPa. To get densified ceramics, the two pressed pellets were sintered at 700 °C for 3 h and 1350 °C for 5 h, giving ceramics with mean grain sizes about 30 nm and 1–2 μm, respectively. The 30 nm ceramic has a density of 68 ± 3 % and will be called STOnm ceramic. The micrograin ceramic has a density of 87 ± 3 % and will be called STOμm. Some of the as-prepared 15 nm powder was annealed at 700 °C and the resulting powder was compacted at room temperature with a uniaxial pressure of a few tens of MPa. It results in a pellet of 30 nm grain size with 30–40 % density. This third sample will be called STOnm compacted powder. The grain size distribution of the powder and ceramics, ~10% around its mean, was measured by scanning electron microscopy. X-ray and neutron diffraction and Raman scattering have been performed to characterize the structural properties.[21] It was found that in both STOnm and STOμm, the rotation of the TiO_6 octahedra cages takes place around 170 K, a temperature much higher than $T_a = 105$ K in the single crystal. This temperature difference partly originates from the strong internal strains arising from ball milling in the ZrO_2 bowl.

III. HRS AT ROOM TEMPERATURE

Figure 1 shows the backscattering HRS spectra of STOnm, STOμm, and STO single crystal (SC) at room temperature. Only TO modes are active in the single crystal for a scattering geometry with **q**//[100], while a weak activity of the LOs is allowed for **q**//[111].[22] This provides the LO3 contribution in the inset. LO1 and LO2 are not shown because they are embedded under the strong TO2 and TO3 modes nearby. In the ceramics, the direction of **q** integrates over all the crystallographic directions and both TOs and LOs are active.

The TO and LO components of the three polar F_{1u}-symmetry vibrations are observed, together with the nonpolar silent F_{2u} mode. This constitutes the full set of vibrations in the $Pm\bar{3}m$ cubic structure. A weak structured background has been removed from the STOnm spectra. For the two others, Fig. 1 reproduces the raw data, emphasizing the more favorable situation of HRS as compared to Raman where the spectral responses are embedded under a very strong and structured background. This is particularly true for TO1 at low frequency, whose spectral response is fully isolated in HRS. The soft mode also benefits from a very favorable Bose-Einstein population factor and largely dominates the hyper-Raman spectra. It broadens when decreasing the grain size (∞ in SC, 1–2 μm in STOμm, and ~30 nm in STOnm) with an almost constant frequency at maximum. The hyper-Rayleigh line at $\omega = 0$ is filtered by the Notch filter which in addition provides the spectral shape a "top-hat" structure when the signal is strong

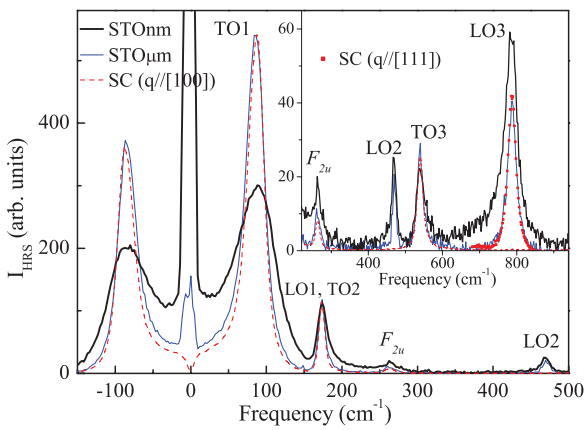

FIG. 1. (Color online) Backscattering HRS spectra of STO ceramics, and in STO single crystal (SC) with **q**//[100] (TO only) and **q**//[111] (LO3 in the inset). The spectra have been recorded with the Notch filter but without the confocal setup, explaining the rather high elastic level in the ceramics. The inset zooms on the high-frequency modes.

(see STOμm spectrum) or a dip when the contribution is small (SC). The strong increase of the elastic contribution with grain size at room temperature is assigned to an increasing concentration of frozen defects per unit volume, likely polar, localized in the grain boundaries.

The inset zooms on the high-frequency excitations. The frequencies of all the modes but TO1 are very close whatever the grain size and are also very similar to the IR ones.[12] The line shapes remain narrow with an asymmetry developing in the gap between the TO-LO companions of the two highest frequency doublets. The additional excitations on the high-frequency tail of TO2 and TO3 arise from distorted regions, probably in grain boundaries where one expects a large concentration of frozen polar defects. The asymmetry seems more pronounced for the LOs, possibly owing to their coupling with the macroscopic electric field through the electro-optic contribution.[23,24] The energy carried by these modes is very weak and when the grain size decreases their spatial extension eventually reduces, but not necessarily their lifetime. Therefore, TO2 and TO3 in ceramics are likely localized within grains even for smallest sizes. This could explain the quasiconstant homogeneous linewidth of TO2 and TO3 when grain size reduces, as is qualitatively suggested by the overlap of the spectral responses on their low-frequency side.

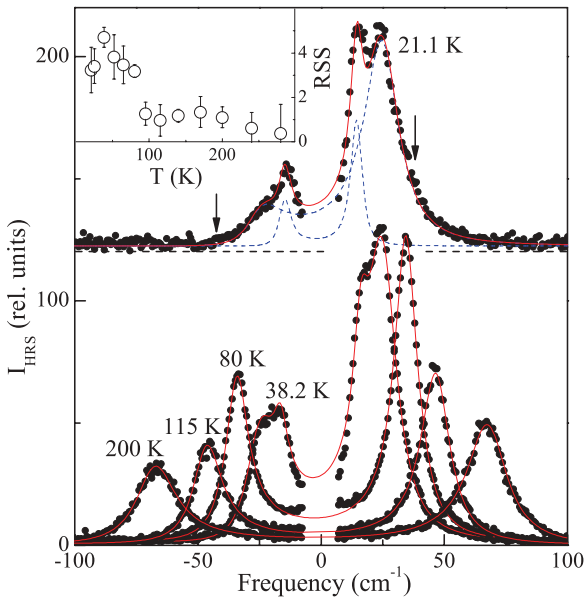

FIG. 2. (Color online) HRS spectra from the soft mode of STOμm ceramic and their fits. The spectra at 21.1 K has been shifted up by 120 counts/15 mn for visibility. The inset shows the normalized residual squared sums (RSS) of the fits (see text).

IV. THE SOFT MODE

A. Fitting procedure

Low-temperature experiments have been performed in a ^{4}He cooling stage ("Microstat," Oxford Instruments) working by conductive heat transfer. In order to limit local heating at the sample due to the incident radiation, the peak power was reduced at low temperature to its lower acceptable value, 35 W, leading to an average power of $\sim$10 mW. However, the simultaneous fitting of the Stoke and anti-Stoke lines revealed a gradient between the temperature of the sensor and that of the sample at low temperature. Therefore, below 80 K, the sample temperature at the scattering volume has been obtained from the simultaneous fit of the Stokes and anti-Stokes soft-mode responses. The latter has been performed by a convolution between the apparatus function and one or two Bose normalized damped harmonic oscillators (DHO) of general formula $I_{\rm HRS} = A_{\rm HRS}[n(\omega)+1]\,\Gamma\omega\omega_0^2/[(\omega^2-\omega_0^2)^2+\Gamma^2\omega^2]$. $n(\omega)$ is the population factor, $A_{\rm HRS}$ is an amplitude factor, ω_0 its frequency, and Γ its damping (full width at half maximum, FWHM).

Figure 2 shows a series of hyper-Raman spectra obtained in the STOμm sample. In that frequency window, the scattering mainly arises from the soft polar transverse optic mode (TO1). Polar vibrations are always active in HRS ensuring that the scattering mostly arises from undistorted regions. The raw HRS spectra unambiguously reveal a splitting of TO1(F_{1u}) into E_u and A_{2u} components at low temperature similar to the behavior of STO single crystal.[13] To our knowledge this has not been evidenced before in a STO ceramic with micrometer grain size, confirming further the high sensitivity of HRS with regard to low-lying polar excitations.

The spectra have been fitted with one DHO down to 100 K while two DHOs were required for temperatures below. Despite an increased number of free fitting parameters in the latter case, the quality of the fits degrades. This can be qualitatively observed on the raw data at 21.1 K and 38.2 K, for which the fit hardly accounts for both the stiff slope at low frequency and the dip between the two modes. These departures can be quantitatively evidenced for example when plotting the residual squared sum of the fitted spectra defined as $\mathrm{RSS}(T) = N(T)\times\sum_\omega[I_{\rm HRS}(\omega,T) - I_{\rm fit}(\omega,T)]^2/I_{\rm fit}(\omega,T)$, where $I_{\rm HRS}(\omega)$ and $I_{\rm fit}(\omega)$ are the experimental data and their fits, respectively, and $N(T)$ is a prefactor essentially accounting for the normalization by the counting time. When looking carefully to the spectra one possibly observes a vanishingly small contribution that peaks around 33 cm^{-1} at 21.8 K (arrows in Fig. 2). The latter can tentatively be attributed to the lowest E_g-symmetry vibration. The mode is normally forbidden in HRS but it could be activated either by structural distortions at grain boundaries[11] or by a coupling with the TO1 soft mode,[11,25] or both. Regarding its very low HRS efficiency, a fit with three modes appears very ambitious. However our trials show that it is by no means sufficient to fully account for the increase of RSS at low temperature. A more likely origin could be the frequency dispersion of TO1 arising from a mixing with its LO counterpart when the mode propagates along arbitrary directions, or from an anisotropy of the TO1 dispersion surface below T_a. The angular averaging over all crystallite orientations could naturally give rise to broad and dissymmetric spectral responses. The fact that the fitting quality is very good at high temperature and degrades when the modes split suggests that the vibrational anisotropy produced by the tetragonal distortion would be the dominant effect. Structural disorder can also provide a natural explanation for the inhomogeneous broadening below $\sim$100 K. In that case, it would indicate that the antiferrodistortive transition induces additional structural distortions in the grains.

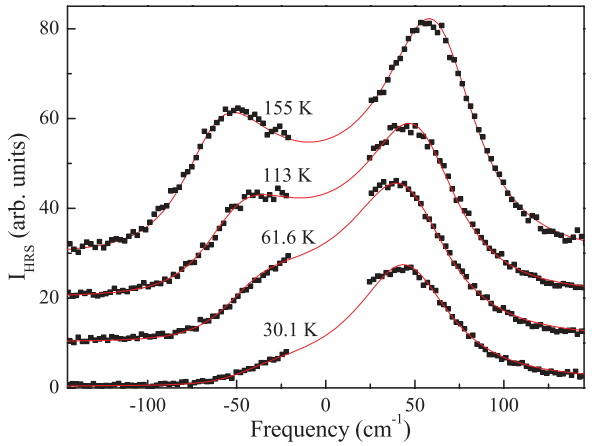

FIG. 3. (Color online) HRS spectra from the soft mode of STOnm ceramic and their fits. For clarity, the spectra at 61.6 K, 113 K, and 155 K have been shifted up by 10, 20, and 30 units, respectively.

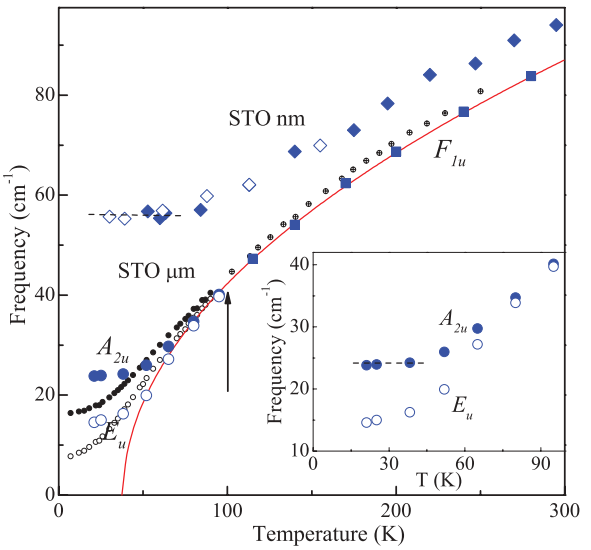

FIG. 4. (Color online) Temperature dependence of the soft mode in STOnm (top symbols) and STOμm (bottom symbols). Empty and filled diamonds correspond to STOnm ceramic and to the compacted powder, respectively. The dots are the data in the single crystal taken from Ref. 13. The inset zooms on the TO1 splitting at low temperatures in STOμm.

Whatever the origin, this additional broadening leads to an overestimated value of the mode frequency ω_0 in a fit with a DHO. In the extreme case where this broadening effect becomes prominent, such a fitting procedure can lead to an apparent hardening of the soft mode at lowest temperatures. For temperatures below 100 K, it thus makes sense defining the frequency of the spectral responses by the peak maxima $\omega_{\max} = \sqrt{(\omega_0^2 - \Gamma^2/2)}$ rather than by ω_0. For ST0μm the difference $\omega_0 - \omega_{\max}$ is negligible at 100 K and reaches at most $+3$ cm^{-1} and $+0.6$ cm^{-1} at 21 K for the A_{2u} and E_u modes, respectively.

Low resolution HRS spectra of TO1 in the nanograin STOnm ceramic are shown in Fig. 3. Owing to a higher sensibility to incident radiation giving rise to sample breaking, the spectra have been recorded at different places in the sample. This prevents intensity calibration and may also explain the slightly larger spread of the results as compared to the micrograin sample. As already observed in Raman,[26,27] TO1 is much more broad for nanograin samples, and its frequency saturates at a higher value on cooling. As no splitting is observed within the experimental resolution, the fits have been done using one single DHO down to lowest temperatures. The agreement is very good without any noticeable anomaly in the RSS values.

B. Soft-mode splitting

Figure 4 summarizes the T dependence of the soft-mode frequency obtained in the different STO samples. Although the maximum frequency of STOnm is very close to that of STOμm at room temperature (Fig. 1), their DHO frequencies ω_0 are different due to a much larger width in the former.

The data in the nanograin ceramic (STOnm) are superposed on those of the compacted powder, revealing that for such grain size and such grain manufacturing, sample density and thermal treatments only produce weak effects on the soft-mode behavior. It also indicates that for those samples, the effective medium approximation likely does not apply for HRS although the excitation wavelength is about 30 times greater than the grain size. Finally, the frequency decreases on cooling and saturates to an almost constant value of 56 cm^{-1} below $\sim$60 K.

The results in STOμm are at lower frequency. The splitting of the F_{1u}-symmetry vibration (filled squares) into A_{2u} (filled circles) and E_u (open circles) components below $\sim$100 K (arrow) is clearly reproduced by the fit. Our data overlap those of the bulk material[13] (black dots) at high temperature, with however a small downshift of $\sim$1 cm^{-1}. This effect is real and can be observed directly on the raw spectra at room temperature (Fig. 1). The data above T_a = 105 K have been fitted with a Curie-Weiss law, $\omega_{TO1}^2 = C(T - T_0)$, with $C = 5.38$ cm^{-2} K^{-1} and $T_0 \simeq 38.18 \pm 0.5$ K. Finally, the modes saturate at low temperature at higher frequency than in the single crystal, with an almost flat temperature dependence of the A_{2u}-symmetry vibration below $\sim$40 K (inset).

The soft-mode behavior presented in Fig. 4 is different from the usual Raman and IR description. In the two latter spectroscopies, the spectra have always been analyzed using one single mode, while all the HRS experiments we performed so far in micrograin STO ceramics revealed a splitting (more or less pronounced) of TO1 at low temperature. Raman suffers from spectroscopic limitations at low frequency (weak signal, strong background) and most likely, the splitting is a too subtle effect to be observed. However, the different scattering processes involved for polar modes in hyper-Raman and Raman discussed above could also possibly give rise to different spectral shapes. Comparing HRS with IR is not straightforward because of the very different excitation wavelengths. In HRS the latter is of the same order of magnitude as the grain size, while wavelengths in the THz range are much larger (from 100 μm to 1000 μm in the soft-mode frequency domain). The splitting of TO1 into E_u- and A_{2u}-symmetry excitations in STOμm constitutes a very

local observation, and suggests that EMA does not apply for HRS in micrometer grain size samples. On the contrary, EMA applies for IR and within the core-shell model the polar mode frequencies relate to an effective permittivity through the Lyddane-Sachs-Teller relation.[12] In that case it is possible that one expects a single IR soft-mode response.

The phenomenological theory developed to lowest order in φ for STO single crystal predicts that the TO splitting, defined as $\Delta\omega_{TO}^2 = \omega_{A_{2u}}^2 - \omega_{E_u}^2$, is proportional to the spontaneous strain $c/a - 1$, the latter being also proportional to the square of the primary order parameter φ^2.[8] The causal link between the tilting angle and the tetragonal distortion originates from the steric effect which imposes that the strontium cage expand along one fourfold axis when the oxygen atoms move out-of-phase from their face-centered position. Below the transition, both motions conspire to minimize the change of the unit cell volume. A linear coupling between these two degrees of freedom, $\varphi^2 \propto c/a - 1$, has experimentally been observed in many perovskite single crystals exhibiting an improper ferroelastic transition (for STO, see, e.g., Ref. 13).

Assuming a linear coupling, and given the values at lowest temperature $\varphi_{\mu m} \simeq 2.45^\circ$ (Ref. 21) and $\varphi_{\text{bulk}} \simeq 2^\circ$,[1,28] respectively, one finds the ratio $(\varphi_{\mu m}/\varphi_{\text{bulk}})^2 = 1.50$ which compares well with $(\Delta\omega_{TO}^2)_{\mu m}/(\Delta\omega_{TO}^2)_{\text{bulk}} = 1.66$ obtained from the present data. This shows that the proportionality constant is similar in both materials, and confirms the conclusion of Ref. 21 that the TiO_6 tilting angle φ is greater in our microceramic than in the bulk material. It also explains the greater TO splitting in our microceramic, 350 cm^{-2} as compared to $\sim$210 cm^{-2} in the bulk sample at 21 K. Though $\Delta\omega_{TO}^2$ and φ^2 linearly relate at low temperature, they exhibit completely different temperature behaviors, as shown in Fig. 5. In STOμm, the two quantities have been superposed at low temperature according to the above estimation, but the TO1 splitting, and consequently $c/a - 1$, decreases much faster than φ^2 on heating, emphasizing a nonlinear coupling between the two quantities. As neutron diffraction data below 170 K are satisfactory refined with a $I4/mcm$ crystal structure,[21] the intermediate region between 170 K and $\sim$100 K could be characterized by a very weak tetragonal distortion, whose

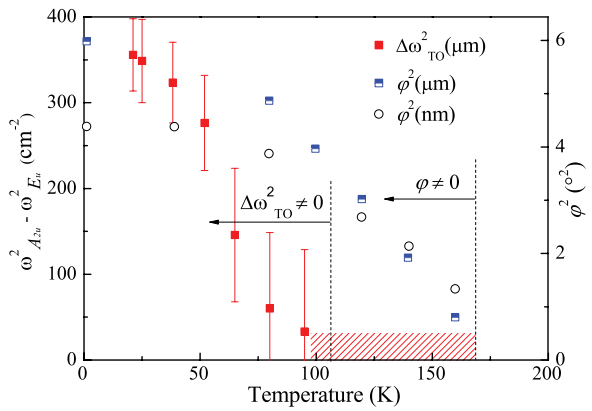

FIG. 5. (Color online) Soft-mode splitting $\Delta\omega_{TO}^2 = \omega_{A_{2u}}^2 - \omega_{E_u}^2$ in STOμm, and squared TiO_6 rotation angle (φ^2) of STOμm and STOnm ceramic. The TO splitting cannot be extracted in the dashed region. The angle values read on the right scale and are reproduced from Ref. 21.

value is beyond the hyper-Raman detection limit. The latter is estimated by the shadowed region in Fig. 5. The large temperature gap between T_a and $\sim$170 K, the temperature at which φ starts growing, is likely a signature of the high strain field the shell imposes on the core grain, and could give a natural explanation for such a strong nonlinear coupling. Indeed, the nature and the geometry of a strain field (e.g., at interfaces) can possibly lead to more complex coupling mechanisms than those usually expected.[29,30] In our microceramic, the behavior somehow appears intermediate between STO under hydrostatic pressure and STO thin films. In the former, the coupling is linear ($c/a - 1 \propto \phi^2$) with a pressure-dependent coupling constant.[31,32] In the latter, tetragonality ($c \neq a$) is observed till very high temperature owing to the clamping to the substrate, but neither c nor a, and therefore $c/a - 1$, are affected by the growth of φ at the transition leading to a perfect decoupling.[33] However, contrary to thin films which can become ferroelectrics,[34] the monotonous increase of the dielectric constant down to lowest temperatures in our ceramic ensures that the strain imposed by the shell to the core grain is not sufficient or does not have the appropriate symmetry to stabilize long-range ferroelectric order. Finally, it is worth noting that the way the primary order parameter couples to the spontaneous strain in STO ceramics likely depends on the sample synthesis method and thermal treatments. Indeed, in samples synthesized with commercial starting powder of STO, the TiO_6 tilt angle develops at a temperature much closer to T_a than in our sample.[11]

C. Disorder-induced broadening

The linewidths of TO1 are shown in Fig. 6. Before discussing the results, we identify below four types of

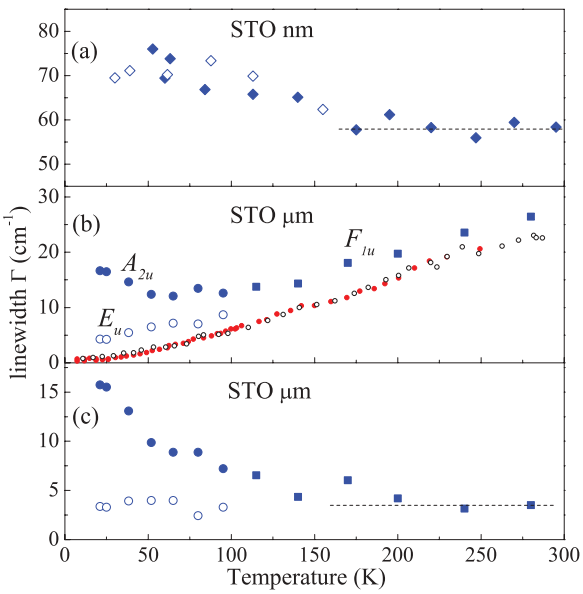

FIG. 6. (Color online) Full width at half maximum of the soft-mode damping. (a) In STOnm. Empty and filled diamonds correspond to data in the ceramic and in the compacted powder, respectively. (b) In STOμm (squares and circles), and in the bulk [black (Ref. 13) and red (Ref. 14) dots]. (c) Anharmonicity-free damping in STOμm (see text).

competing broadening mechanisms. As the soft mode in the bulk material remains highly underdamped down to the lowest temperatures, we excluded the viscous damping process that could occur close to a displacive phase transition, as for example in $BaTiO_3$.[35] The two first mechanisms are homogeneous processes and are modeled by the DHO spectral response. The following two are inhomogeneous and when sufficiently efficient, they lead to asymmetric or Gaussian spectral line shapes.

Damping can first originate from interactions of phonons in the thermal bath. This anharmonic process often applies in perfect crystals and leads to a line narrowing on cooling. It largely dominates in STO single crystal [Fig. 6(b)]. In ceramics, the linewidth can be affected by the reduction of the phonon lifetime due to grain-size and grain-boundary effects. Local inhomogeneities can also give rise to a distribution of the mode frequency. This third contribution is usually more pronounced for localized excitations which in disordered materials generally vibrate at high frequencies. The fourth line-broadening mechanism has an experimental origin and has already been mentioned before. It is associated with the angular averaging over the phonon dispersion surface when looking in polycrystals.

The linewidth of STOμm first narrows on cooling with a slope similar to that of the bulk sample, showing that anharmonicity still dominates [Fig. 6(b)], which is not the case for STOnm whose linewidth is almost flat [Fig. 6(a)]. For the micrograin sample, it is thus worthwhile defining an anharmonicity-free quantity, obtained by subtracting the bulk values from the raw data [Fig. 6(c)]. Therefore Fig. 6(a) should be compared to Fig. 6(c), and indeed, one observes very similar trends, at least above $\sim$100 K. Excluding anharmonicity, this suggests a common origin for the broadening processes in the two samples. At high temperature, the spectral responses are DHO-type (Fig. 2 and Fig. 3) favoring a damping mechanism due to the reduction of the grain size (type 2 above) in the flat region. The width is much larger in STOnm owing to smallest grains limiting much more efficiently the phonon lifetime. The linewidth of the two ceramics then slightly increases upon cooling. It starts around $\sim$160 K, the temperature at which the TiO_6 octahedra starts tilting. As no anomaly at T_a is observed in the bulk sample, we assign this effect in the ceramics to the presence of structural distortions generated by the growth of φ.

Below T_a, the broadening of the A_{2u}-symmetry component of STOμm becomes so important that it makes a minimum in its temperature curve. It correlates with the RSS anomaly and to the onset of asymmetry of the doublet spectral shape (Fig. 2). It is not possible to conclude whether this inhomogeneous broadening arises preferentially from the anisotropy of the phonon sheet (type 4) or from structural distortions (type 3) induced by the growth of the tetragonal axis, but most likely both mechanisms contribute. According to the above, this effect is weaker in STOnm owing to a smaller spontaneous strain.

It is also worth noting that the width of the E_u component is much less affected by these effects than that of A_{2u}. The former mimics the anharmonic behavior of the bulk sample, with approximately the same constant offset whatever the temperature. As the ferroelectric soft mode involves preferentially the titanium atoms, it is tempting to attribute this difference in behavior to an increasing disorder anisotropy on cooling, with a larger Ti-site disorder along the c-tetragonal axis than in the (a,b) plane.

Finally, the results in the nanograin ceramic and in the compacted powder are very similar [Fig. 6(a)], confirming thereby that thermal treatments influence only weakly the soft-mode properties. This and the above discussion also indicate that contrary to IR which probes the effective medium, the soft mode measured in HRS is sensitive to local structural details.

V. CONCLUSION

Hyper-Raman scattering has been performed in a micro and nano STO ceramic sintered from the same starting nanometric powder, and in a compacted powder arising from the same source. The full set of vibrations expected in the $Pm\bar{3}m$ cubic phase are observed, that is, the three polar F_{1u}-symmetry modes and the *silent* F_{2u}-symmetry vibration. Instrumental improvements have opened the possibility to measure the vibrations down to $\sim$8 cm^{-1} in perovskite ceramics. In STO, the hyper-Raman signal lies on a very weak background allowing therefore a very accurate vibrational spectroscopy.

For example, a splitting of the soft TO1 into E_u- and A_{2u}-symmetry modes is clearly observed in the micrograin sample. Its unusual temperature dependence is indicative of a nonlinear coupling between the TiO_6 tilt angle squared, φ^2, and the spontaneous strain $c/a - 1$. Such behavior possibly arises from the strain field the shell imposes on the core grain and one therefore expects that it is strongly dependent on the synthesis route and grain size. These very interesting issues should motivate further theoretical and experimental works.

The soft-mode line shape is influenced by several mechanisms, including for example the reduction of the phonon lifetime due to grain size effect. The analysis suggests that the growth of the primary order parameter φ around 170 K induces local distortions. Moreover, the strong difference in the temperature behaviors of the E_u and A_{2u} modes in the micrograin ceramic is assigned to an anisotropic disorder on the Ti site on cooling below T_a. Regarding the symmetry of the modes, it is proposed that this disorder is greater along the c axis than in the (a,b) plane.

Finally, our results demonstrate that HRS is sensitive to local vibrational and structural properties, mostly those of the core grains. As the soft mode is intimately related to the permittivity, it is thus likely that the spectroscopy probes the *microscopic* dielectric properties, which are probably close to the ultimate intrinsic ones. It differs from the *macroscopic* permittivity measured by standard dielectric tools and probably also from that extracted from IR experiments, whose value is limited, e.g., by the low dielectric constants in the grain boundaries and the density of the ceramic.

ACKNOWLEDGMENTS

The work was supported by the ANR project (FERROENERGY) and the Region Languedoc-Roussillon ("OMEGA" Platform). One of us (B.H.) would like to thank E. Courtens and R. Vacher for fruitful discussions.

*Current address: European Synchrotron Radiation Facility, 6 Rue Jules Horowitz, 38043 Grenoble Cedex, France.

[1]K. A. Müller, W. Berlinger, and F. Waldner, Phys. Rev. Lett. **21**, 814 (1968); H. Thomas and K. A. Müller, *ibid.* **21**, 1256 (1968).
[2]G. Shirane and Y. Yamada, Phys. Rev. **177**, 858 (1969).
[3]M. Sato, Y. Soejima, N. Ohama, A. Okazaki, H. J. Scheel, and K. A. Müller, Phase Trans. **5**, 207 (1985).
[4]K. Hirota, J. P. Hill, S. M. Shapiro, G. Shirane, and Y. Fujii, Phys. Rev. B **52**, 13195 (1995).
[5]K. A. Müller and H. Burkard, Phys. Rev. B **19**, 3593 (1979).
[6]J. G. Bednorz and K. A. Müller, Phys. Rev. Lett. **52**, 2289 (1984).
[7]J. Hemberger, M. Nicklas, R. Viana, P. Lunkenheimer, A. Loidl, and R. Böhmer, J. Phys.: Condens. Matter **8**, 4673 (1996).
[8]H. Uwe and T. Sakudo, Phys. Rev. B **13**, 271 (1976).
[9]M. Itoh, R. Wang, Y. Inaguma, T. Yamaguchi, Y-J. Shan, and T. Nakamura, Phys. Rev. Lett. **82**, 3540 (1999).
[10]T. K. Song, J. Kim, and S.-I. Kwun, Solid State Commun. **97**, 143 (1996).
[11]J. Petzelt, I. Gregora, I. Rychetsky, T. Ostapchuk, S. Kamba, P. Vanek, Y. Yuzyuk, A. Almeida, M. R. Chavez, B. Gorshunov, M. Dressel, S. Hoffmann-Eifert, and R. Waser, J. Europ. Ceram. Soc. **21**, 2681 (2001).
[12]J. Petzelt, T. Ostapchuk, I. Gregora, P. Kuzel, J. Liu, and Z. Shen, J. Phys.: Condens. Matter. **19**, 196222 (2007).
[13]A. Yamanaka, M. Kataoka, Y. Inaba, K. Inoue, B. Hehlen, and E. Courtens, Europhys. Lett. **50**, 688 (2000).
[14]H. Vogt, Phys. Rev. B **51**, 8046 (1995).
[15]V. N. Denisov, B. N. Marvin, and V. B. Podobedov, Phys. Rep. **151**, 1 (1987).
[16]A. Al-Zein, J. Hlinka, J. Rouquette, and B. Hehlen, Phys. Rev. Lett. **105**, 017601 (2010).
[17]A. Al-Zein, J. Hlinka, J. Rouquette, A. Kania, and B. Hehlen, J. Appl. Phys. **109**, 124114 (2011).
[18]G. Simon, B. Hehlen, R. Vacher, and E. Courtens, Phys. Rev. B **76**, 054210 (2007).
[19]Olympus microscope modified by Optique Peter Corp. for combining hyper-Raman and Raman spectroscopies: http://www.optiquepeter.com.
[20]OptiGrate Corp.: http://www.optigrate.com.
[21]J. M. Kiat, C. Bogicevic, P. Gemeiner, A. Al-Zein, F. Karolak, N. Guiblin, F. Porcher, B. Hehlen, Ll. Yedra, S. Estradé, F. Peiró, and R. Haumont, Phys. Rev. B **87**, 024106 (2013).
[22]A. Al-Zein, B. Hehlen, J. Rouquette, and J. Hlinka, Phys. Rev. B **78**, 134113 (2008).
[23]H. Vogt, Phys. Rev. B **38**, 5699 (1988).
[24]B. Hehlen, G. Simon, and J. Hlinka, Phys. Rev. B **75**, 052104 (2007).
[25]E. Courtens, G. Coddens, B. Hennion, B. Hehlen, J. Pelous, and R. Vacher, Phys. Scr., T **49B**, 430 (1993).
[26]J. Petzelt, T. Ostapchuk, I. Gregora, D. Nuzhnyy, I. Rychetsky, K. Maca, and Z. Shen, Ferroelectrics **363**, 227 (2008).
[27]T. K. Song, J. Kim, S.-I. Kwun, C. J. Kim, and J.-J. Kim, Physica B **219**, 538 (1996).
[28]J. M. Kiat and T. Roisnel, J. Phys.: Condens. Matter **8**, 3471 (1996).
[29]M. A. Carpenter and E. K. H. Salje, Eur. J. Mineral. **10**, 693 (1998).
[30]E. K. H. Salje, Phys. Chem. Minerals **35**, 321 (2008).
[31]M. Guennou, P. Bouvier, J. Kreisel, and D. Machon, Phys. Rev. B **81**, 054115 (2010).
[32]E. K. H. Salje, M. Guennou, P. Bouvier, M. A. Carpenter, and J. Kreisel, J. Phys.: Condens. Matter **23**, 275901 (2011).
[33]Feizhou He, B. O. Wells, Z-G. Ban, S. P. Alpay, S. Grenier, S. M. Shapiro, Weidong Si, A. Clark, and X. X. Xi, Phys. Rev. B **70**, 235405 (2004).
[34]H. W. Jang, A. Kumar, S. Denev, M. D. Biegalski, P. Maksymovych, C. W. Bark, C. T. Nelson, C. M. Folkman, S. H. Baek, N. Balke, C. M. Brooks, D. A. Tenne, D. G. Schlom, L. Q. Chen, X. Q. Pan, S. V. Kalinin, V. Gopalan, and C. B. Eom, Phys. Rev. Lett. **104**, 197601 (2010).
[35]H. Vogt, J. A. Sanjurjo, and G. Rossbroich, Phys. Rev. B **26**, 5904 (1982).